Defective potassium channel Kir2.1 trafficking underlies Andersen-Tawil syndrome.

Saïd Bendahhou[*], Matthew R. Donaldson[*], Nikki M. Plaster[*], Martin Tristani-Firouzi[†], Ying-Hui Fu[‡], and Louis J. Ptácek[*,§]

[*]Department of Human Molecular Biology and Genetics; [†]Division of Pediatric Cardiology [‡]Department of Neurobiology and Anatomy; [§]Department of Neurology and Howard Hughes Medical Institute, University of Utah, Salt Lake City, Utah, USA.

Running Title: *KCNJ2* mutations associated with Andersen's syndrome

Correspondence to Saïd Bendahhou

Université de Nice Sophia Antipolis

Institut de Pharmacologie Moléculaire et Cellulaire

660 Route des Lucioles

Sophia-Antipolis 06560 Valbonne – France

Phone: (33) 4 93 95 77 41   Fax: (33) 4 93 95 77 08   Email: bendahhou@ipmc.cnrs.fr

Text pages: 23   # Figures: 8   # Table: 0

Words in Abstract: 203

Abbreviations: ATS, Andersen-Tawil syndrome; EGFP, enhanced green fluorescent protein

Summary

Andersen-Tawil syndrome is a skeletal and cardiac muscle disease with developmental features caused by mutations in the inward rectifier K^+ channel gene *KCNJ2*. Patients harboring these mutations exhibit extremely variable expressivities. To explore whether these mutations can be correlated with a specific patient phenotype, we expressed both wild-type (WT) and mutant genes cloned into a bi-cistronic vector. Functional expression in human embryonic kidney 293 cells showed that none of the mutant channels express current when present alone. When co-expressed with WT channels, only construct V302M-WT yields inward current. Confocal microscopy fluorescence revealed three patterns of channel expression in the cell: 1) mutations D71V, N216H, R218Q, and pore mutations co-assemble and co-localize to the membrane with the WT and exert a dominant-negative effect on the WT channels; 2) mutation V302M leads to channels that lose their ability to co-assemble with WT and traffic to the cell surface; 3) deletions 95-98 and 314-315 lead to channels that do not traffic to the membrane but retain their ability to co-assemble with WT channels. These data show that Andersen-Tawil syndrome phenotype may occur through a dominant-negative effect as well as through haplo-insufficiency and reveal amino acids critical in trafficking and conductance of the inward rectifier K^+ channels.

Introduction

Andersen-Tawil syndrome (ATS) is a rare autosomal dominant disorder caused by mutations in the inward rectifier potassium channel gene *KCNJ2* which encodes the inward rectifier potassium channel Kir2.1 protein. Two features of this disease have made this gene of high interest to scientists: i) patients suffer from both skeletal muscle periodic paralysis and cardiac arrhythmia, a unique feature in ion channel diseases; ii) patients exhibit developmental problems such as cleft palate, low-set ears, short stature and development features in the limbs (clinodactyly, syndactyly, brachydactyly) (1-3). While the first feature can be easily understood because of the contribution of Kir2.1 to membrane excitability in both tissues, it is still unknown how this channel contributes to craniofacial, limb, and axial skeletal development.

The inward rectifier potassium channel (Kir) family is subdivided into seven members according to the extent of amino acid sequence homology (4). The predicted transmembrane topology of the Kir family is shown in Figure 1. The protein consists of two membrane-spanning segments, namely M1 and M2, a pore-forming loop between the two transmembrane segments, and amino- and carboxy-termini located intracellularly. Four subunits co-assemble in a homo- or hetero-multimeric manner to form a channel (5). The *KCNJ* genes are widely expressed in the body. They can be found in muscle (*KCNJ2*, *KCNJ11*), heart (*KCNJ2*, *KCNJ3*, *KCNJ5*, *KCNJ11*), brain (*KCNJ3*, *KCNJ6*, *KCNJ9*, *KCNJ11*), epithelial (*KCNJ1*, *KCNJ2*), and many other tissues (6-12). Mutations in the *KCNJ* gene family produce three inherited disorders in man and one in mouse. In *KCNJ1* (Kir1.1), mutations have been associated with Bartter's syndrome (13), an autosomal recessive disorder characterized by hypokalemia and salt wasting. Mutations in *KCNJ11*

3

(Kir6.2) and the associated protein SUR1 have been linked to the syndrome of persistent hyperinsulinemic hypoglycemia in infancy (PHHI) (14,15). A mutation in Kir3.2 (GIRK2) produces the *weaver* phenotype in mice in an autosomal recessive manner (16). This disease results in a loss of neurons and severe ataxia. Most recently, we reported nineteen mutations in the *KCNJ2* gene causing ATS (17-19). The clinical manifestations in ATS patients are very variable suggesting that different mutations may account for different phenotypes.

Early expression of mutations in *Xenopus* oocytes led us to suggest that all ATS mutations cause ATS through a dominant-negative mechanism. To better understand the pathogenesis of this disease, we carried out mammalian cell expression studies of previously identified mutations D71V, 95-98, S136F, G144S, N216H, R218Q, G300V, V302M, E303K, and 314-315. While most of the mutations appeared to have a dominant negative effect on the kir2.1 channel, we observed near-normal currents when mutation V302M was co-expressed with WT. Furthermore, confocal microscopy fluorescence data implicate several amino acid residues, previously unknown, essential for channel assembly, trafficking, and membrane expression. This work provides insights into the complex functional domains of the C-terminus of Kir2.1 as well as ATS pathogenesis.

Materials and Methods

Mutagenesis

Human cardiac *KCNJ2* was obtained in the plasmid pBluescript KS (-) as a gift from Carol Vandenberg. Mutagenic primers were used to generate all point mutations and deletions with the GeneEditor kit (Promega) according to the manufacturer recommendations and as previously described (17). WT cDNA was fused to Ds red fluorescent protein (DsRed) and all mutant clones (D71V, S136F, G144S, N216H, R218Q, G300V, V302M, E303K, amino acid deletion 95-98, DSWLF, and deletion 314-315, SY) were fused to enhanced green fluorescent protein (EGFP) and subcloned in the pDsRed and pEGFP vectors. These clones were subsequently PCR-amplified using primers flanked with *NheI* and *EcoRI* enzymes for the first cloning site or *NotI* restriction enzyme for the second cloning site, and subcloned into the pIRES vector (BD Biosciences). Mutant clones were subcloned in the first multi-cloning site and the WT-RFP cDNA was subcloned in the second multi-cloning site. All PCR products and final constructs were sequenced to ensure fidelity.

Tissue culture and Electrophysiology

Human embryonic kidney (HEK) 293 cells were grown and transfected using calcium-phosphate precipitation technique (20) and as previously described (21).

Current recordings were conducted in the whole-cell configuration (22) at room temperature (22˚C), using an Axopatch 200B amplifier (Axon Instrument Inc., Foster City, CA). Data acquisition and analysis were performed with pClamp6 (Axon Instrument Inc., Foster City, CA) and Igor Pro (WaveMetrics Inc., OR) programs.

Pipettes (Kimax) of 0.8-1.5 MΩ were prepared using a Sutter P-87 puller (Novato, CA) and heat-polished prior to use. The pipette tip potential was adjusted to zero for each experiment. To minimize space clamp problems due to the electrical coupling between HEK 293 cells, only isolated cells with a soma size of 10-30 μm were selected for recordings. Twenty-four to 36 hours after transfection, the culture media was removed and replaced with a bathing solution containing: NaCl 135 mM, KCl 5 mM, MgCl$_2$ 1mM, glucose 10 mM, and HEPES 10 mM (pH 7.3). The pipette solution was: KCl 140 mM, MgCl$_2$ 2 mM, EGTA 1mM, and HEPES 10 mM (pH 7.3). Currents were elicited by 200-ms pulses applied in 10-mV increments to potentials ranging from -120 mV to +30 mV from a holding potential of -60 mV.

Confocal microscopy

Fluorescence microscopy was performed with a Nikon Eclipse TE300 inverted microscope and images were captured and manipulated with a CoolSNAP camera and software. The confocal is a BioRad MRC 1024 and the software is LaserSharp version 3.2.

Western Immunoblot

Untransfected and transiently-transfected HEK 293 cells were harvested and lysed in 10 mM Tris, pH 7.5, 0.1 mM EDTA, 0.1 mM EGTA, 0.5% SDS, 0.1 mM β-mercaptoethanol, containing 2 μg/ml of each of the protease inhibitors leupeptin, aprotinin, and pepstatin. Aliquots of 20 μl were electrophoresed on 8% SDS-polyacrylamide gels and transferred to nitrocellulose membranes (Millipore, Bedford,

MA). Blots were incubated with anti-EGFP (1:1,000) antibodies, and the proteins of interest were visualized using an ECL detection system (Amersham Biosciences).

Results

Andersen-Tawil syndrome mutants do not produce current in HEK293 cells

In order to correlate functional expression data with confocal microscopy fluorescence imaging, *KCNJ2* wild type (WT) or mutant cDNAs (D71V, G144S, N216H, R218Q, G300V, V302M, E303K, amino acid deletion 95-98, and 314-315) were fused to DsRed or EGFP at the C-terminal end and subcloned into the pIRES vector (Fig. 1). All constructs were subsequently introduced and expressed in HEK293 cells using whole cell patch clamp technique. Only cells transfected with WT-DsRed cDNA exhibited K^+ conductance when cells were subjected to potentials ranging from –120 mV to +30 mV (Fig. 2). The current-voltage relationship of the WT-EGFP or WT-DsRed clones is identical to published data on *KCNJ2* gene expressed in HEK293 cells (23). This suggests that the KCNJ2 protein product retained its normal functional properties when fused to EGFP or DsRed such as subunit assembly, trafficking, and rectification. However, there was no current expressed in HEK293 cells 24 hours or even 36 hours post-transfection when mutant cDNAs were used. All currents recorded have the same amplitude and characteristics of those recorded from mock-transfected cells (-117 ± 22 pA at –120 mV, n= 8).

ATS mutants exert a dominant-negative effect on WT channels

Because ATS is an autosomal dominant trait and KCNJ2 channels can assemble as homo-tetramers, we introduced WT and mutant channels in the same cell using a bi-cistronic expression vector. A pIRES plasmid was constructed that directs the co-expression of two proteins with the first protein fused to EGFP (mutant cDNA) and the second protein

fused to DsRed (WT cDNA). An encephalomyocarditis virus internal ribosomal entry site (IRES) mediates translational initiation from this 3' cassette, and a cytomegalovirus promoter drives bi-cistronic transcripts expression. Current recorded from cells transfected with the construct containing WT-GFP/WT-RFP had an amplitude higher (-2788 ± 355 pA at –120 mV; n= 8) than that recorded from cells transfected with WT-GFP (-2347 ± 316 pA at –120 mV; n= 8) or WT-DsRed only, suggesting that transcripts are produced from both sites. When mutant channels (mutant-EGFP) were used at the first site and WT-DsRed at the second site in the same vector no current was detected from all constructs except V302M-GFP/WT-DsRed (-700 ± 135 pA at –120 mV; n= 8) (Figure 2). These results suggest that all ATS mutants exert a dominant-negative effect on WT channels except the V302M mutation, which may cause the disease through a haplo-insufficiency mechanism.

Channel assembly and trafficking are targeted in Andersen-Tawil syndrome

To understand how these mutants exert their dominant-negative effect and why the V302M substitution leads to ion conductance when co-expressed with WT channels, all constructs fused to either EGFP or DsRed were expressed in HEK293 cells on a cover slip and confocal microscopy study was conducted. We used single constructs to monitor channel distribution in the cell and double constructs (mutant-EGFP/WT-DsRed) to monitor both channel distribution and assembly. The same constructs used in electrophysiology were used for confocal microscopy imaging. All single constructs showed that mutant channels had a cellular distribution similar to that of WT channels except 95-98-EGFP, V302M-EGFP and 314-315-EGFP. These three mutants

exhibited a scattered pattern of expression (Figure 3). Double constructs with mutant-EGFP in the first site and WT-DsRed in the second site allowed us to investigate how our mutants interact with WT KCNJ2. Figure 4 shows the distribution of the WT and mutant channels in HEK293 cells. While D71V, G144S, N216H, R218Q, G300V, and E303K (-EGFP) co-localize to the membrane with the WT-DsRed producing a yellow color,   95-98-EGFP and   314-315-EGFP co-localize in the cytoplasm with WT-DsRed and also produce a yellow color (Figure 4). Interestingly, V302M channels do not co-localize with WT (green fluorescence in the cytoplasm) and only WT-DsRed is expressed in the membrane.

According to the crystal structure of the a bacterial potassium channel (KirBac1.1), which has structure representative of the Kir family, amino acids 95-98 are found in the outer helix (24). A deletion in this segment may cause misfolding of the protein and, consequently, retention in the endoplasmic reticulum (ER) or degradation. Amino acids 302, 314, and 315 are located in the complex functional C-terminus domain of Kir2.1. For   314-315 channels, the yellow color seems to be mainly localized to the cytoplasm. This indicates that these mistrafficked mutant channels retain their ability to co-assemble with the WT-DsRed protein, thus trapping functional WT-DsRed protein in the cytoplasm. Finally, the V302M substitution seems to affect both channel trafficking and assembly since the V302M-EGFP channels are found in the cytoplasm and the WT-DsRed channels are located in the membrane (Figure 4). This expression pattern further supports our electrophysiological data showing that only the V302M-EGFP/WT-DsRed construct was able to give rise to potassium conductance, due to the free WT-DsRed subunits that were unable to co-assemble with the mutant subunits.

In order to identify the relative contribution of the deleted amino acids at positions 314 and 315, we mutated each of them to Alanine and introduced them into the pIRES vector with and without WT-DsRed in the second site. Confocal microscopy images of transfected HEK293 cells showed that Y315A substitution caused a more dramatic effect than substitution S314A (Figure 5). The WT and mutant channels seem to be sequestered together in the cytoplasm.

Involvement of C-terminal residues of Kir2.1 in trafficking

Our study of ATS mutations revealed three amino acid residues in the C-terminal domain of the Kir channels that may be part of a binding motif essential for channel trafficking. This region is indeed well conserved among Kir family members (Fig. 6B). To test our hypothesis, we extended our mutagenesis studies to residues surrounding the amino acids involved in ATS. We performed alanine scanning mutagenesis of most of the residues from 290 to 325. All Kir clones were constructed in the first cloning site of the pIRES vector in-frame with the EGFP. After cell transfection, confocal microscopy images were taken to assess the localization of the channels. Our data show that mutations of residues L316, E319, I320, L321, and W322 show an intracellular distribution pattern (Fig. 6A) very similar to that observed for either the deletion S314-Y315 (Fig. 4) or the substitutions S314A-GFP and Y315A-GFP (Fig. 5). Although these channels retain their ability to co-assemble with WT, they seem to be sequestered in the cytoplasm.

11

Discussion

ATS is characterized by periodic paralysis, ventricular dysrhythmias with long-QT (LQT) and skeletal developmental abnormalities. We have linked the *KCNJ2* gene to ATS and identified mutations in families with ATS phenotypes (17-19). Three of these mutations are located in the N-terminus (R67W, D71V/N and T75R), one deletion occurs in the first transmembrane segment M1 (95-98), three mutations occur in the pore region (S136F, G144S andG146D) and the remaining mutations reside in the C-terminus of the Kir 2.1 channel (P186L, R189I, N216H, R218Q/W, G300V/D, V302M, E303K, R312C and 314-315). Combining functional expression and confocal microscopy imaging, we were able to identify amino acids that abolish channel function, affect homomeric channel assembly, and play a role in channel trafficking.

D71V, N216H, R218Q, R218W, G300V, and E303K mutant channels seem to co-assemble with the Kir2.1-WT channels and to co-localize to the plasma membrane in HEK293 cells. In so doing, the non-functional mutant protein likely "poisons" the Kir2.1 channel tetramer. We anticipate that several mechanisms underlie channel silencing since these amino acid residues localize to different functional domains of the Kir2.1 protein as shown on the crystal structure of the Kirbac1.1 (Fig. 7). Changes occurring in the pore region likely alter the conformation of the pore or its potassium ion selectivity to produce a non-functional channel as has already been shown for a Kir3.2 mutation causing the *weaver* phenotype in mice (16), and those introduced to the pore of the channel (25). The D71V mutation does not alter channel assembly or trafficking or seem to be degraded, suggesting that the slide helix plays a role in the Kir2.1 channel gating. Alternatively,

mutations occurring in the N-terminus cytoplasmic region of the Kir2.1 may interfere with the correct insertion of segment M1 into the membrane (26).

Mutations in the C-terminus of the protein produce diverse effects on the whole cell current confirming multiple functions of this domain. This is expected since the distal part of the channel starting at the M2 segment has been implicated in rectification, sensitivity to phosphorylation, PIP$_2$ binding, PSD-95/SAP-90 binding, and has an ER export motif (23,27-32). While N216H, R218Q, R218W, G300V, E303K, and 314-315 produce no current when expressed alone or with the normal WT channel, V302M does not produce any measurable current when expressed alone but yields an inwardly rectifying current in the presence of WT channels in the same cell. By altering this site, the mutant channels could not reach the plasma membrane. This may be due to a trafficking defect or a consequence of channel misfolding. Only channels composed of free WT reached the membrane and could produce detectable current (Fig. 2).

Using anti-GFP antibodies, we were able to detect 2 major bands at 75 and 90 kDa for all fusion constructs except that of the V302M mutation that showed only 75 kDa band (Fig. 8). This finding may indicate instability of the V302M mRNA or protein. Alternatively, this mutation may cause misfolding of Kir2.1 leading to incomplete post translational modifications. Further characterization of this mutation is necessary to elaborate the associated mechanism. In any case, our data suggest that residue V302 is part of a critical motif responsible for proper channel folding and may produce ATS through a haplo-insufficiency mechanism.

Deletion 314-315 also lost its ability to traffic to the membrane, but did not alter subunit assembly. WT subunits were trapped in the cytoplasm by the mutant subunits to

form non-functional channels. Alanine scanning mutagenesis of these two amino acids showed that substitutions at residue 315 may have a more pronounced effect on channel trafficking than those at residue 314 (Fig. 5). These data also support our hypothesis that this region is part of an essential binding motif for channel trafficking.

Mutations N216H, R218Q, G300V, and E303K do not seem to affect trafficking or assembly of the Kir2.1, but still produce non-functional channels. These amino acids reside close to a region thought to be involved in rectification and in phosphatidylinositol-4,5-bisphosphate (PIP_2) binding (33-37). Residue 216 and R218 have been shown to be involved in Kir2.1-PIP_2 interactions. PIP_2 seems to be ligand for a Kir2.1 channel activation (34). Channels that interact strongly with the PIP_2 are constitutively active at negative potentials and contribute to setting rest membrane potential (38,39). Additionally, we have recently shown that PIP2-binding residues of the Kir2.1 are common targets of mutations causing ATS (18). Mutations in PIP_2-related residues accounted for over 60% of reported *KCNJ2* probands.

It is difficult from these experiments to determine the exact contribution of each residue in the C-terminal domain of the protein to channel trafficking or assembly, despite the availability of the crystal structure. The C-terminus of the kir2.1 contains the ER export sequence FCYENE and trafficking-related acidic clusters EEDDSE at positions 374-379 and 386-391 respectively (28,40). Our data show that these two sequences are not sufficient for efficient surface expression and that additional trafficking signals are required. Our alanine scanning mutagenesis identified two amino acid clusters (residues 314-316 and 319-322), and further supports the idea of complex protein folding of the residues surrounding S314-Y315 to create a three-dimensional interaction site

essential for Kir trafficking. This is supported by the crystal structure of Kibac1.1 which shows beta sheets formed with these residues. Either other Kir domains are required or other kir2.1 partner proteins are necessary for surface expression of these channels. Alternatively, residues located between amino acids 310 and 330 may be involved in channel heteromerization as suggested recently for these channels (41).

ATS patients exhibit the triad of muscle weakness, cardiac ectopy, and developmental abnormalities. The excitability features of this disease can be understood as Kir2.1 is expressed in the membrane of excitable cells and plays an essential role in maintaining the resting membrane potential and shaping the cardiac action potential (39). Mutations preventing proper expression of Kir2.1 in the membrane can understandably interfere with normal cell excitability and cause the repolarization defects of this disease. Our data indicate ATS can be caused by such a mechanism and implicate novel regions of Kir2.1 essential for membrane expression. In addition, our findings may have implications for other *loci* underlying ATS as previous studies have indicated mutations in other genes likely cause nearly 40% of diagnosed cases of ATS. Genes encoding proteins which facilitate membrane expression of Kir2.1 by interacting with the trafficking regions of the C-terminus or localize Kir2.1 to specific regions of the membrane may be involved. Recently, mutations in the first non-ion channel, non-accessory subunit (Ankyrin-B), were found to cause a form of long QT syndrome, LQT4 (42). This adaptor protein anchors ion channels to the T-tubules and a loss of its function seems to cause long-QT by resultant disruption in localized ion channel function. Another study has shown that filamin-A (actin-binding protein) may interact with Kir2.1 protein at the C-terminus domain (43). It is reasonable to speculate that mutations in interacting,

trafficking, or anchoring proteins might cause unexplained cases of ATS.

Experiments are underway to determine the role of the amino acid residues in the C-terminus and for a potential binding motif that may shed light on inward rectifier potassium channel modulation, assembly and trafficking. Our data clearly identify residues crucial for KCNJ2 channel trafficking that can be useful to understanding the involvement of KCNJ2 in the developmental pattern seen in ATS patients.

Legends to Figures

Figure 1: Topology of the Kir family and mutations associated with the *KCNJ2* gene

[A] Two helical structures form the membrane-spanning segments (M1 and M2), the pore region P, and two intracellular fragments (N and C termini) form a subunit that oligomerize to form a channel. All ATS missense mutations (filled circles, R67W, D71V/N, T75R, S136F, G144S, G146D, P186L, R189I, N216H, R218Q/W, G300V/D, V302M, E303K, R312C) and deletions (triangles, 95-98 and 314-315) are represented on the channel. **[B]** pIRES constructs used for HEK293 cells transfection. WT cDNA was fused to DsRed fluorescent protein (DsRed) and mutant clones (D71V, T75R, S136F, G144S, N216H, G300V, V302M, E303K, amino acid deletion 95-98, SWLF, deletion 314-315, SY) were fused to enhanced green fluorescent protein (EGFP) and subcloned in the pDsRed and pEGFP vectors. These clones were subsequently PCR-amplified, and subcloned into the pIRES vector. Mutant clones were subcloned in the first site and the WT-RFP cDNA was subcloned in the second site.

Figure 2: Functional expression of ATS mutations in HEK293 cells

Current voltage relationship obtained from HEK293 cells transfected with either single construct or with a pIRES construct containing mutant channels at the first cloning site and WT KCNJ2 cDNA in the second cloning site. Mutant cDNA were constructed in-frame with EGFP and WT cDNA was in-frame with DsRed. Cells were voltage clamped in the whole cell configuration. Currents were elicited by holding the cells to -60 mV and depolarized to various test potentials from -120 to +30mV for 200 ms. Peak currents were

measured for each test potential and plotted as a current-voltage curve. Values are mean ± SEM from 8 individual cells.

Figure 3: ATS mutations affect Kir channel distribution

Confocal microscope fluorescent images (x100) of HEK293 cells expressing EGFP alone, DsRed alone, KCNJ2 wild type, and ATS mutations fused to EGFP. Notice that fluorescence is localized to the membrane for WT, D71V, G144S, N216H, R218Q, G300V, and E303K. Notice also that fluorescence is sparsely distributed inside the cells for constructs 95-98, V302M, and 314-315.

Figure 4: Consequences of ATS mutations on KCNJ2 trafficking

HEK293 cells were transfected with pIRES constructs containing mutant-EGFP in the first multi-cloning site and WT-DsRed in the second multi-cloning site. Confocal microscope images (x100) were taken with overlapping green and red fluorescence.

Figure 5: Contribution of residues 314 and 315 to KCNJ2 function

Amino acids Serine 314 and Tyrosine 315 were mutated to Alanine and introduced into the pIRES vector in the first multi-cloning site with WT-DsRed in the second multi-cloning site. Both mutant cDNA constructs were fused to EGFP at their 3'end. Confocal microscope images (x100) of transfected HEK293 cells were taken with overlapping green and red fluorescence to show the distribution of WT and ATS mutated channels in the same cell.

Figure 6: Involvement of the C-terminal domain in Kir trafficking

[A] Confocal microscopy fluorescence images from HEK293 cells transfected with *KCNJ2* (WT or mutant) fused to EGFP. Residues were mutated to Alanine. Note normal distribution of the channel at the cell membrane for WT and N318A channels, and the cytoplasmic distribution of all other constructs. **[B]** Alignment of KCNJ2 primary structure with other proteins from the inward rectifier family. Blue characters denote of amino acid residues that altered Kir2.1 distribution in the cell. Lower case letters denote of conservative amino acid changes, and "." Denotes of non-conservative changes.

Figure 7: Localization of ATS mutations on the Kirbac1.1 crystal structure

KCNJ2 residues 71, 95 to 98, 136, 144, 216, 218, 300, 302, 303, and 314-315, that align with Kirbac1.1 residues 50, 74 to 77, 104, 112, 179, 181, 259, 261, 262, and 273-274 respectively, are shown for four subunits (A) or for one subunit only (B). The same residues for one of the subunit are labeled in red.

Figure 8: Expression pattern of Kir2.1 fusion proteins

Protein extracts from HEK 293 cells transfected with EGFP alone, WTKir2.1-EGFP, D71V-EGFP, 95-98-EGFP, 314-315-EGFP, and mock transfected were analyzed by western immunoblotting using anti-GFP antibody. When EGFP is expressed alone, it shows a molecular mass of 30 kDa.

References

1.   Andersen, E. D., Krasilnikoff, P. A., and Overvad, H. (1971) *Acta Paediatr. Scand.* **60,** 559-564.

2.   Tawil, R., Ptacek, L. J., Pavlakis, S. G., DeVivo, D. C., Penn, A. S., Ozdemir, C., and Griggs, R. C. (1994) *Ann. Neurol.* **35,** 326-330.

3.   Sansone, V., Griggs, R. C., Meola, G., Ptacek, L. J., Barohn, R., Iannaccone, S., Bryan, W., Baker, N., Janas, S. J., Scott, W., Ririe, D., and Tawil, R. (1997) *Ann. Neurol.* **42,** 305-312.

4.   Doupnik, C. A., Davidson, N., and Lester, H. A. (1995) *Curr. Opin. Neurobiol.* **5,** 268-277.

5.   Yang, J., Jan, Y. N., and Jan, L. Y. (1995) *Neuron* **15,** 1441-1447.

6.   Yano, H., Philipson, L. H., Kugler, J. L., Tokuyama, Y., Davis, E. M., Le Beau, M. M., Nelson, D. J., Bell, G. I., and Takeda, J. (1994) *Mol. Pharmacol.* **45,** 854-860.

7.   Raab-Graham, K. F., Radeke, C. M., and Vandenberg, C. A. (1994) *Neuroreport* **5,** 2501-2505.

8.   Stoffel, M., Espinosa, R., 3rd, Powell, K. L., Philipson, L. H., Le Beau, M. M., and Bell, G. I. (1994) *Genomics* **21,** 254-256.

9.   Sakura, H., Bond, C., Warren-Perry, M., Horsley, S., Kearney, L., Tucker, S., Adelman, J., Turner, R., and Ashcroft, F. M. (1995) *FEBS Lett.* **367,** 193-197.

10.   Lesage, F., Fink, M., Barhanin, J., Lazdunski, M., and Mattei, M. G. (1995) *Genomics* **29,** 808-809.

11.   Tucker, S. J., James, M. R., and Adelman, J. P. (1995) *Genomics* **28,** 127-128.

12.   Inagaki, N., Gonoi, T., Clement, J. P. t., Namba, N., Inazawa, J., Gonzalez, G., Aguilar-Bryan, L., Seino, S., and Bryan, J. (1995) *Science* **270,** 1166-1170.

13.   Simon, D. B., Karet, F. E., Rodriguez-Soriano, J., Hamdan, J. H., DiPietro, A., Trachtman, H., Sanjad, S. A., and Lifton, R. P. (1996) *Nat. Genet.* **14,** 152-156.

14.   Thomas, P. M., Cote, G. J., Wohllk, N., Haddad, B., Mathew, P. M., Rabl, W., Aguilar-Bryan, L., Gagel, R. F., and Bryan, J. (1995) *Science* **268,** 426-429.

15.   Thomas, P., Ye, Y., and Lightner, E. (1996) *Hum. Mol. Genet.* **5,** 1809-1812.

16.   Patil, N., Cox, D. R., Bhat, D., Faham, M., Myers, R. M., and Peterson, A. S. (1995) *Nat. Genet.* **11,** 126-129.

17.   Plaster, N. M., Tawil, R., Tristani-Firouzi, M., Canun, S., Bendahhou, S., Tsunoda, A., Donaldson, M. R., Iannaccone, S. T., Brunt, E., Barohn, R., Clark, J., Deymeer, F., George, A. L., Fish, F. A., Hahn, A., Nitu, A., Ozdemir, C., Serdaroglu, P., Subramony, S. H., Wolfe, G., Fu, Y., and Ptacek, L. J. (2001) *Cell* **105,** 511-519.

18.   Tristani-Firouzi, M., Jensen, J. L., Donaldson, M. R., Sansone, V., Meola, G., Hahn, A., Bendahhou, S., Kwiecinski, H., Fidzianska, A., Plaster, N., Fu, Y. H., Ptacek, L. J., and Tawil, R. (2002) *J Clin Invest* **110**, 381-388.

19.   Donaldson, M. R., Jensen, J. L., Tristani-Firouzi, M., Tawil, R., Bendahhou, S., Suarez, W. A., Cobo, A. M., Poza, J. J., Behr, E., Wagstaff, J., Szepetowski, P., Pereira, S., Mozaffar, T., Escolar, D. M., Fu, Y. H., and Ptacek, L. J. (2003) *Neurology* **60**, 1811-1816.

20.   Graham, F. L., and Van Der Eb, A. J. (1973) *Virology* **52,** 456-467

21.   Bendahhou, S., Cummins, T. R., Tawil, R., Waxman, S. G., and Ptacek, L. J. (1999) *J. Neurosci.* **19,** 4762-4771

22.   Hamill, O. P., Marty, A., Neher, E., Sakmann, B., and Sigworth, F. J. (1981) *Pflugers Arch.* **391**(2)**,** 85-100

23.   Kubo, Y., and Murata, Y. (2001) *J. Physiol.* **531,** 645-660.

24.   Kuo, A., Gulbis, J. M., Antcliff, J. F., Rahman, T., Lowe, E. D., Zimmer, J., Cuthbertson, J., Ashcroft, F. M., Ezaki, T., and Doyle, D. A. (2003) *Science* **300**, 1922-1926.

25.   Tinker, A., Jan, Y. N., and Jan, L. Y. (1996) *Cell* **87,** 857-868.

26.   Umigai, N., Sato, Y., Mizutani, A., Utsumi, T., Sakaguchi, M., and Uozumi, N. (2003) *J. Biol. Chem.* (in press).

27.   Wischmeyer, E., and Karschin, A. (1996) *Proc. Natl. Acad. Sci. U. S. A.* **93,** 5819-5823.

28.   Nehring, R. B., Wischmeyer, E., Doring, F., Veh, R. W., Sheng, M., and Karschin, A. (2000) *J. Neurosci.* **20,** 156-162.

29.   Tong, Y., Brandt, G. S., Li, M., Shapovalov, G., Slimko, E., Karschin, A., Dougherty, D. A., and Lester, H. A. (2001) *J. Gen. Physiol.* **117,** 103-118.

30.   Ma, D., Zerangue, N., Lin, Y. F., Collins, A., Yu, M., Jan, Y. N., and Jan, L. Y. (2001) *Science* **291,** 316-319.

31.   Stockklausner, C., Ludwig, J., Ruppersberg, J. P., and Klocker, N. (2001) *FEBS Lett.* **493**, 129-133.

32.   Soom, M., Schonherr, R., Kubo, Y., Kirsch, C., Klinger, R., and Heinemann, S. H. (2001) *FEBS Lett.* **490**, 49-53.

33.   Hilgemann, D. W., and Ball, R. (1996) *Science* **273,** 956-959.

34.   Huang, C. L., Feng, S., and Hilgemann, D. W. (1998) *Nature* **391,** 803-806.

35.   Zhang, H., He, C., Yan, X., Mirshahi, T., and Logothetis, D. E. (1999) *Nat. Cell Biol.* **1,** 183-188.

36.   Chen, L., Kawano, T., Bajic, S., Kaziro, Y., Itoh, H., Art, J. J., Nakajima, Y., and Nakajima, S. (2002) *Proc Natl. Acad. Sci. U. S. A.* **99,** 8430-8435.

37.   Lopes, C. M., Zhang, H., Rohacs, T., Jin, T., Yang, J., and Logothetis, D. E. (2002) *Neuron* **34,** 933-944.

38.   Hille, B. (1992) *Ionic channels in excitable membranes*, 2nd Ed., Sinauer, Sunderland, MA.

39.   Nichols, C. G., and Lopatin, A. N. (1997) *Annu. Rev. Physiol.* **59,** 171-191.

40.   Ma, D., Zerangue, N., Raab-Graham, K., Fried, S. R., Jan, Y. N., and Jan, L. Y. (2002) *Neuron* **33,** 715-729.

41.   Preisig-Muller, R., Schlichthorl, G., Goerge, T., Heinen, S., Bruggemann, A., Rajan, S., Derst, C., Veh, R. W., and Daut, J. (2002) *Proc. Natl. Acad. Sci. U. S. A.* **99,** 7774-7779.

42.   Mohler, P. J., Schott, J. J., Gramolini, A. O., Dilly, K. W., Guatimosim, S., DuBell, W. H., Song, L. S., Haurogne, K., Kyndt, F., Ali, M. E., Rogers, T. B., Lederer, W. J., Escande, D., Le Marec, H., and Bennett, V. (2003) *Nature* **421**, 634-639.

43.   Sampson, L. J., Leyland, M. L., and Dart, C. (2003) *J. Biol. Chem.* (in press).
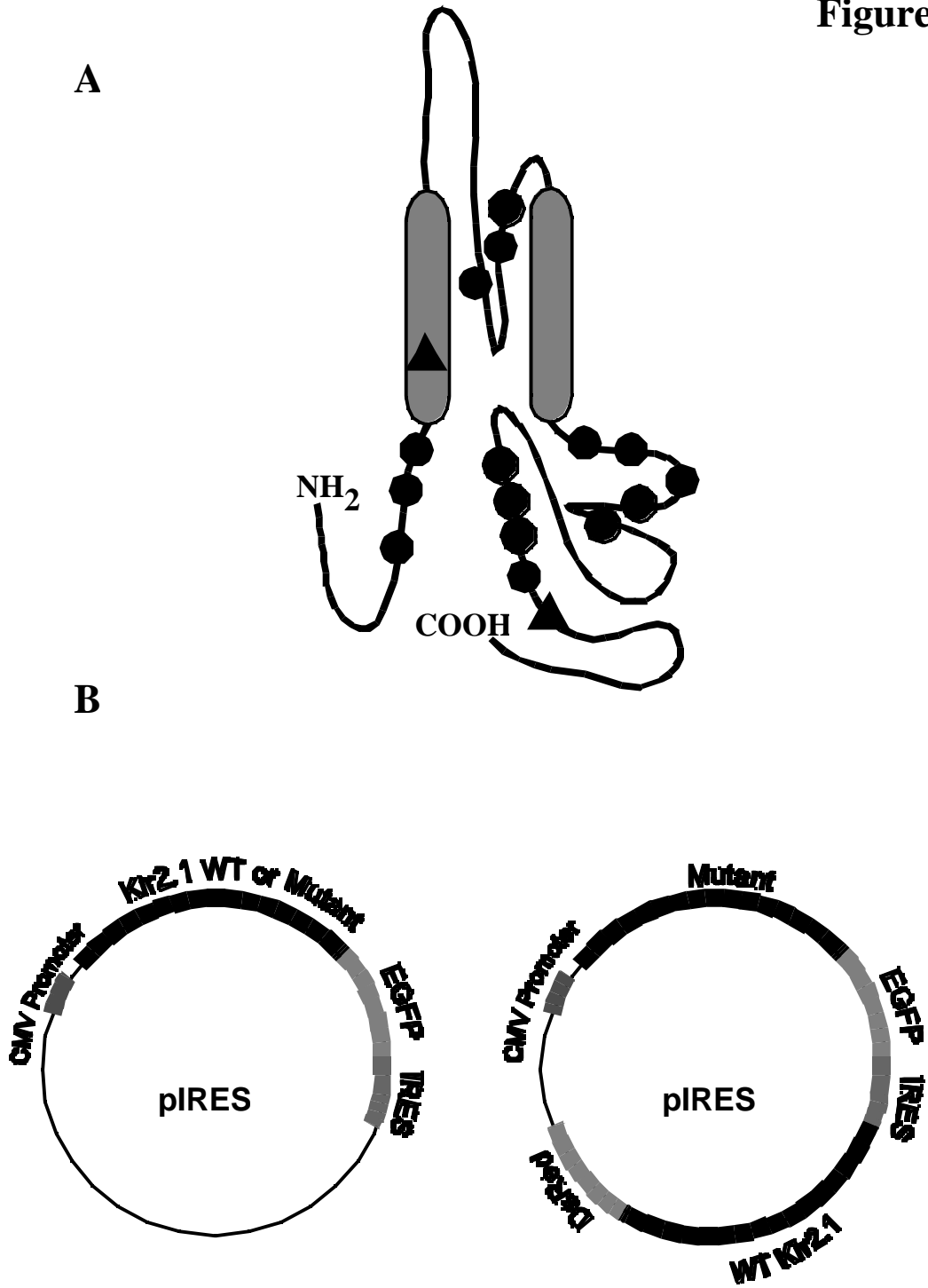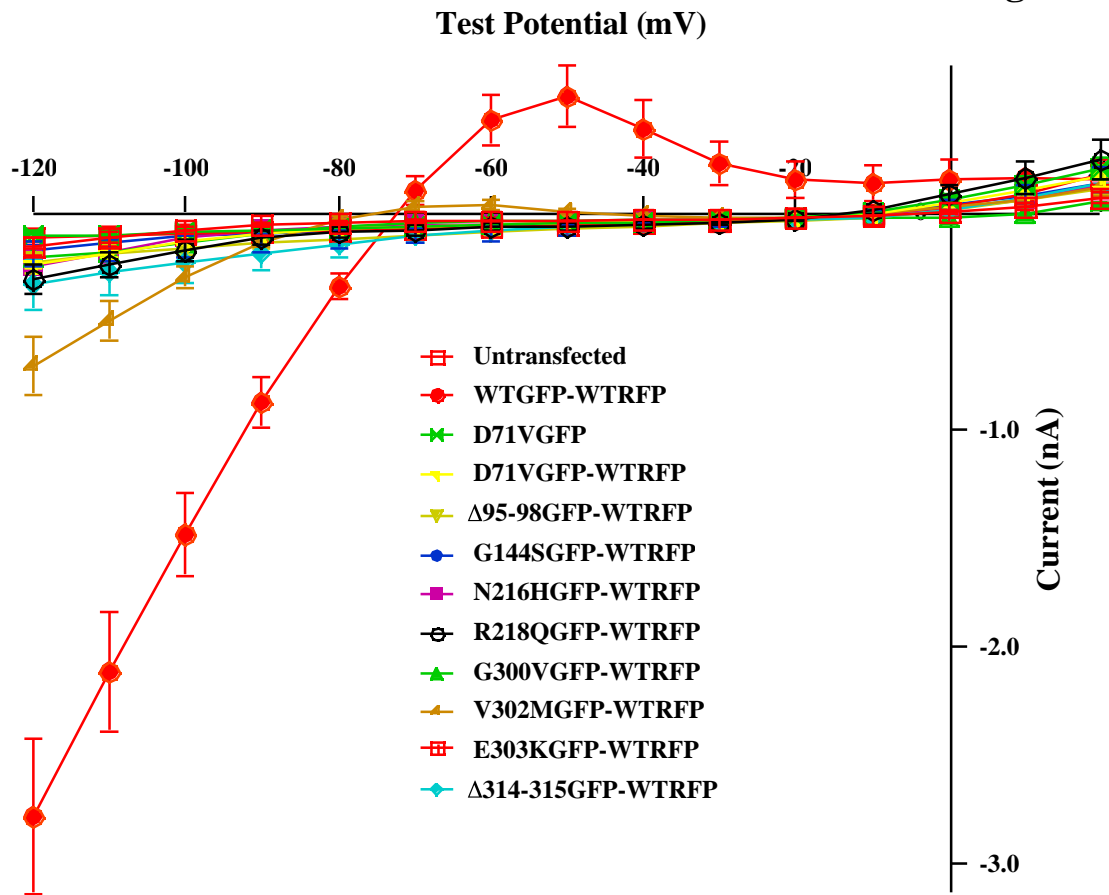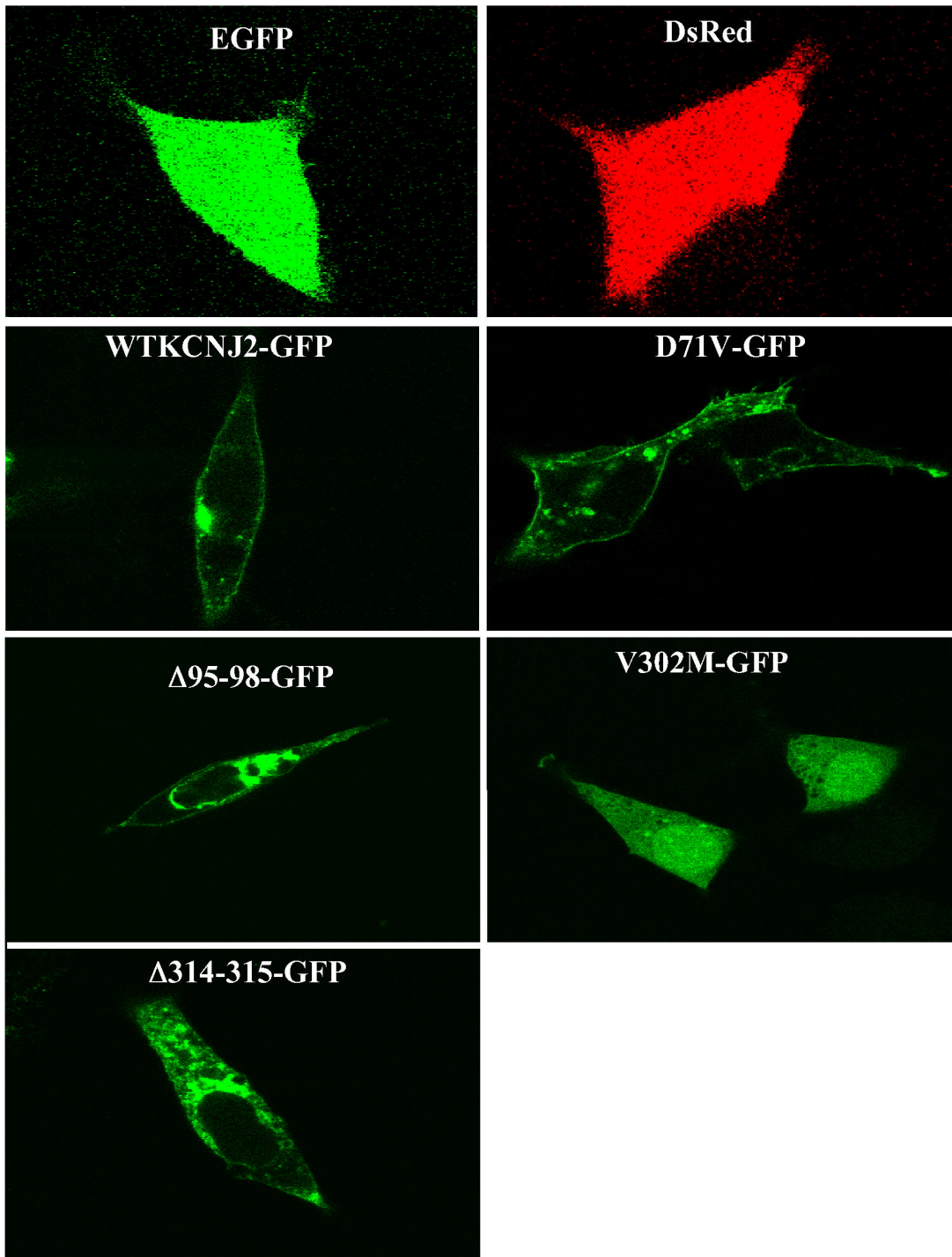
Figure 1

A

B

Figure 2

Figure 3

EGFP

DsRed

WTKCNJ2-GFP

D71V-GFP

Δ95-98-GFP

V302M-GFP

Δ314-315-GFP

Figure 4

Figure 5

S314AGFP

Y315AGFP

S314AGFP-WTDsRed

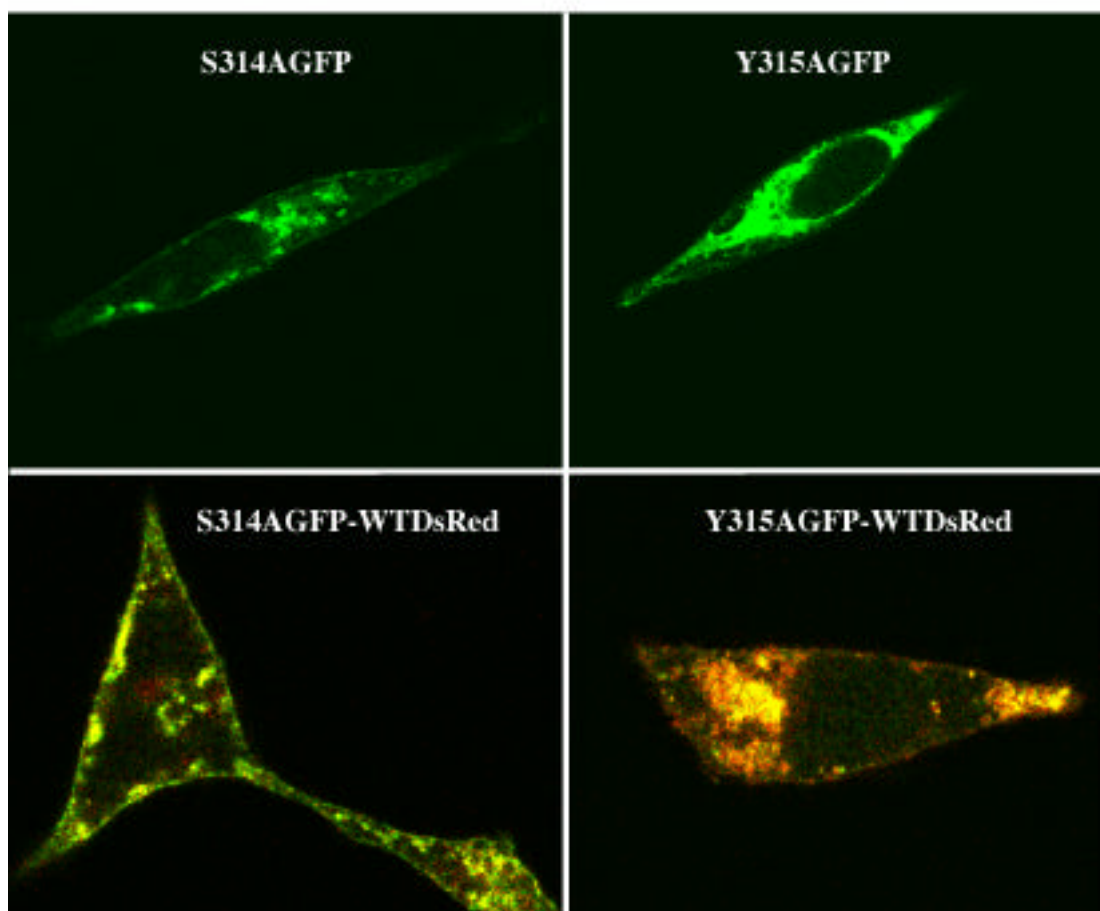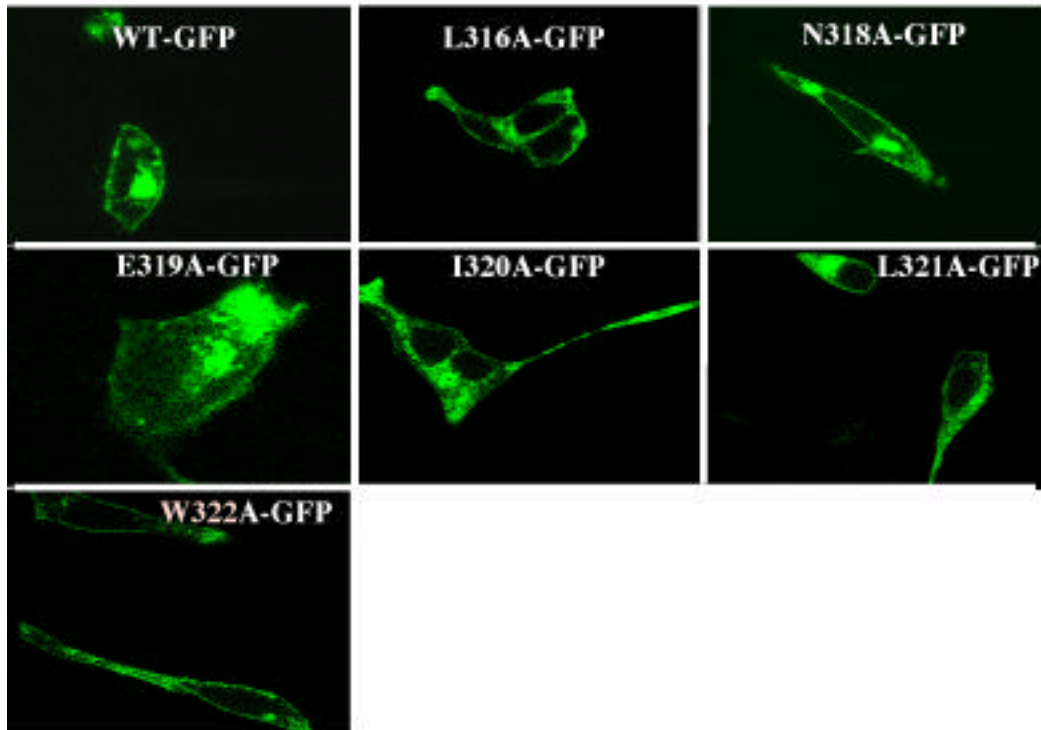Y315AGFP-WTDsRed
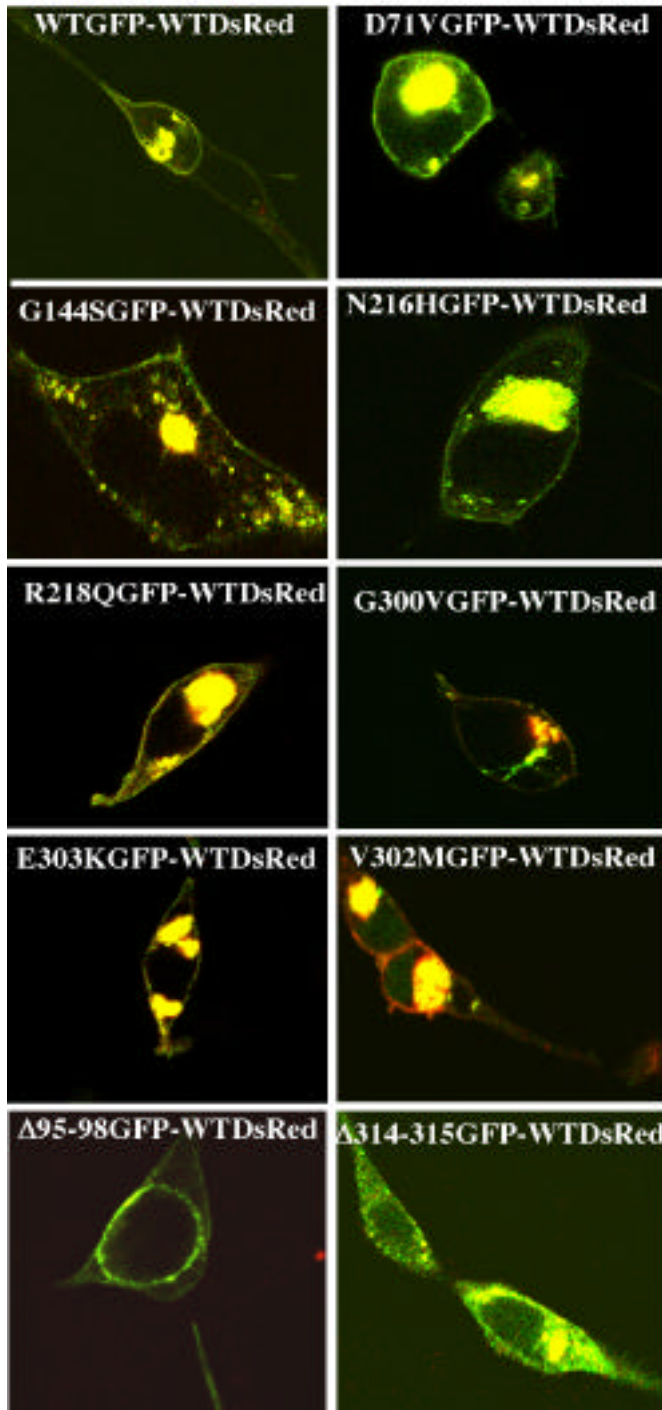
Figure 6

A

B

```
                              314-316    319-322

Kir 2.1   TAMTTQCRSSYLANEILW
Kir 2.2   TAMTTQaRSSYLANEILW
Kir 2.3   TAMTTQaRSSYLAsEILW
Kir 1.1   Ts.T.Q.RtSYv..EvLW
Kir 3.1   TgMT.Q.RtSY..dEvLW
Kir 4.1   Ts.T.Q.RtSYL..EILW
Kir 5.1   Tg.s.Q.RSSYv..EILW
Kir 6.1   TgiTTQ.RtSYiA.EI.W
Kir 7.1   Tg...Q.RtSYL..EIm.
```
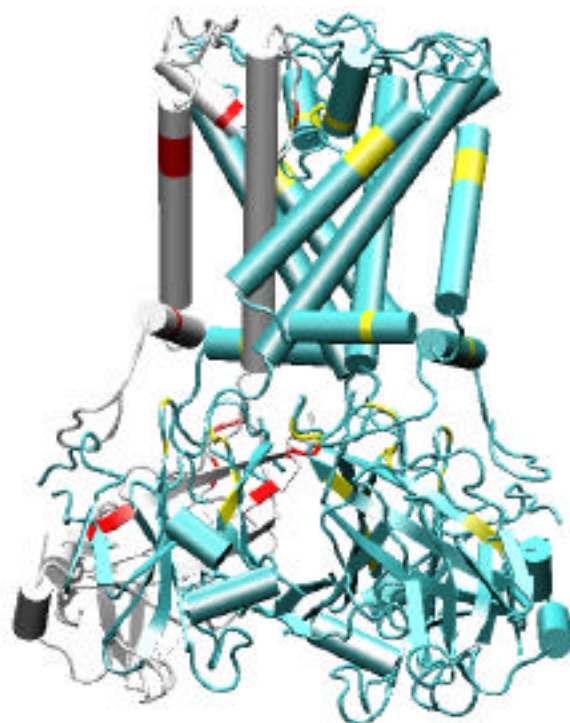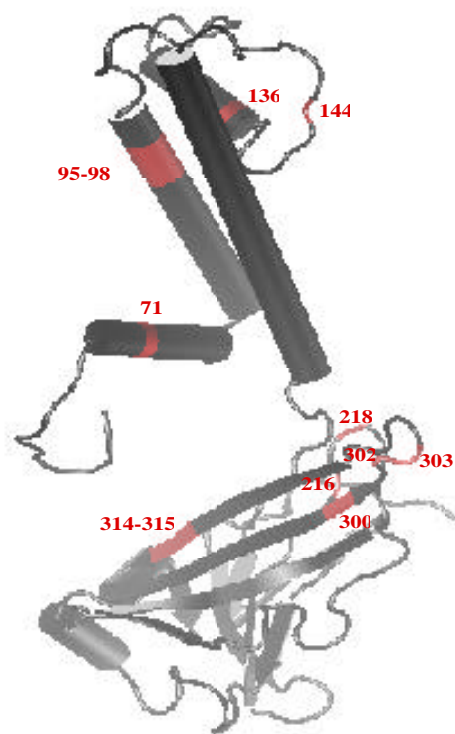
B

Figure 8

GFP   UNTR   WT Δ314-315 V302M Δ95-98 D71V

97 kDa ━━━

66 kDa ━━━

30 kDa ━━━